20

Mapping and quantification of microcirculation features during photodynamic therapy

© A.V. Guryleva¹, T.G. Grishacheva², A.S. Machikhin¹, D.A. Ziganurova^{1,3}, A.S. Beliaeva¹, A.A. Zolotukhina¹, S.G. Chefu², P.V. Luzhnov³, N.N. Petrishchev²

e-mail: guryleva.av@ntcup.ru

Received February 01, 2025 Revised February 10, 2025 Accepted April 07, 2025

Photodynamic therapy is a promising and minimally invasive treatment option for a wide range of skin diseases. The feasibility of mapping and quantifying blood microcirculation parameters simultaneously in the tumor and surrounding tissues during photodynamic therapy using photoplethysmography was investigated to optimize treatment protocols and assess effectiveness. An experimental setup and digital data processing algorithms were developed and outlined. The mapping of changes in back-scattered light intensity and pulse wave parameters related to tissue blood volume and oxygenation was demonstrated in a model animal. The time dependencies of microcirculation features in healthy and tumor tissues during photoactivation and the subsequent recovery period were presented. The limitations of the proposed approach and strategies to address them are described.

Keywords: biophotonics, noninvasive diagnostics, photodynamic therapy, photoplethysmography, digital image processing.

DOI: 10.61011/EOS.2025.05.61650.29-25

1. Introduction

Skin diseases occur in almost a third of the world's population and remain the fourth most common cause of patient disability in the world [1,2]. Photodynamic therapy (PDT), characterized by significant therapeutic and cosmetic effects combined with low invasiveness, high selectivity to pathological tissues and almost complete absence of side effects, is considered to be the clinically demanded and most promising method of treating such diseases [3,4]. The PDT procedure includes the administration of a photosensitizer (PS) to the patient — a light-absorbing compound that accumulates mainly in atypical target cells, and its subsequent photoactivation (PA), which consists in irradiating the pathological area and surrounding healthy tissues with radiation of a certain spectral composition [5].

To determine the optimal PDT protocols and control the effectiveness of treatment in clinical practice, a comprehensive quantitative assessment of the tissue response to photodynamic effects is required [6–8]. In most PDT protocols, the greatest contribution to the therapeutic effect is provided by exposure to the vascular network [9,10], therefore, studying the reaction of the microcirculatory bed to photodynamic effects at all stages of the procedure is the most reliable and informative approach to assessing the result of PDT.

Widely used contact devices based on laser [11] and ultrasonic [12] Doppler flowmetry methods are characterized by the simplicity of the study, however, they require monitoring the force and location of the sensor.

The most informative methods for visualizing the characteristics of the microcirculatory bed in PDT include optical coherence tomography/angiography [13], magnetic resonance imaging [14], confocal microscopy [15], photoacoustic microscopy [16], two-photon microscopy [17]. The implementation of these methods usually requires expensive equipment and significant computing power, which makes it difficult for them to be widely implemented in clinical practice. In addition, they do not monitor blood microcirculation directly during photodynamic exposure. At the same time, early changes in the microcirculatory system have a direct effect on the PDT result [18]. Therefore, the analysis of blood microcirculation during PDT can serve as a source of valuable data for evaluating the effectiveness of protocols and clinical monitoring.

Noninvasive monitoring of blood microcirculation with high spatial and temporal resolution, including during PDT, can be performed using photoplethysmography. This method makes it possible to quantify tissue perfusion based on the analysis of a temporary periodic signal proportional to the intensity of radiation reflected from the skin — photoplethysmograms (PPG) [19], and is used to obtain the shape and quantitative characteristics of the pulse wave of blood microcirculation in solving many biomedical problems [20,21]. Photoplethysmography is used to monitor oxygen saturation, heart rate and respiration, blood pressure, cardiac output, etc. [20,22,23].

¹ STC UI RAS, Moscow, Russia

² Pavlov St. Petersburg State Medical University, St. Petersburg, Russia

³ Bauman Moscow State Technical University, Moscow, Russia

One of the most informative ways to implement tissue research using photoplethysmography is to obtain and analyze the spatial distribution of signals from the PPG and of its parameters [24]. In this case, it is necessary to register a set of images of the studied area for a certain period of time. The analysis can be performed at various scales depending on the type of the imaging optical system. A common approach is to use a photographic lens in the imaging channel, which allows obtaining data on perfusion changes in a wide field of view with spatial resolution in the space of objects of the order of several millimeters [25,26]. When using a microscope, it is possible to analyze small areas of the skin with greater detail, including visualization of the capillary network of the tissue under study — videocapillaroscopy [27–29].

Previously, the authors developed a stand for noninvasive mapping of the capillary network of small skin areas during PDT using photoplethysmography [30]. The purpose of this paper is to study the applicability of the photoplethysmography method for visualization and quantification of individual parameters of blood microcirculation simultaneously in the tumor and in the surrounding conditionally healthy skin areas in case of PDT. To achieve this goal, an experimental bench and an algorithm for processing the data obtained with its help were optimized, tested in an experimental study on a model animal, and their limitations and application prospects were determined.

Materials and methods

Approach used

The proposed approach is based on photoplethysmography, a widely used method for analyzing biological tissues that was first introduced in Ref. [31,32]. Despite improvements in hardware and algorithms for digital processing of recorded PPG over the past decades, the key principles of data analysis remain the same. The signal recorded by the radiation receiver consists of several main components determined by tissue parameters, as well as spatial and temporal low- and high-frequency noise [33,34].

A constant or time-varying component of the signal, often referred to in the literature as a DC-component, is associated with the characteristic of the absorption capacity of tissues such as bones, fat, muscles, and total blood volume [35]. Changes in the intensity of radiation absorption caused by respiration and a corresponding change in oxygenation are often also attributed to this component [36]. component that characterizes changes in the absorption capacity or backscattering characteristics of radiation by internal structures caused by cardiac activity is called the AC-component and is attributed to the useful signal -PPG [37]. The magnitude of these changes corresponds to complex changes in stroke volume, vascular elasticity, transmural pressure, etc. [38]. Typical noise components are additive dark noise of the radiation receiver, spatial unevenness of the radiation receiver sensitivity, aberration

distortion and vignetting, spatial and temporal unevenness of illumination, etc. [39].

The final contribution of various types of tissues and parameters of the peripheral vascular system to the AC and DC-component is determined by the spectral range of the radiation used, the recording mode ("for transmission" or "for reflection"), the localization of measurement, diagnostic volume, etc. [36,40]. The traditional implementation option can be called the use of radiation in the near-infrared spectral range, however, in recent decades, PPG methods have also been developing using illumination in the visible region of the spectrum, usually in green (510-560 nm). This is attributable to the fact that the absorption capacity of blood in the blue-green region is higher than in the red and near-infrared regions. At the same time, the radiation from the green region has a greater penetration depth than the blue one [41,42]. Such features lead to an increase in the depth of modulation of the radiation scattered by the internal structures of the skin in the green area [43,44]. It is shown that such a region is characterized by a lower sensitivity to artifacts of local and global displacements of the studied region in the frame [45].

The main disadvantage of using radiation in this region of the spectrum is the lower depth of penetration into tissues $(0.4-0.9 \,\mathrm{mm} \, [42,46])$, corresponding to the occurrence of the capillary network, characterized by low or absent frequency of fluctuations in its blood filling during the cardiac cycle [47]. However, a number of studies note the similarity of the results obtained in the near-infrared and green regions [48]. The possibility of photoplethysmography and obtaining a pulse wave in the green region of the spectrum is explained in Ref. [47,49] by tissue deformation and changes in capillary density with changes in transmural blood pressure in deeper layers of the skin. Other studies demonstrate the successful application of remote registration of the spatial distribution of the parameters of the PPG in case of usage of radiation from the green region of the spectrum [24,25,50].

The AC-component is most often used and its parameters are analyzed and, if necessary, mapped when describing blood microcirculation using photoplethysmography: the amplitude and width of the pulse wave extracted from the AC-component, the intervals between systolic and diastolic peaks of neighboring pulses, etc. [19,20,50]. One of the approaches to quantifying the amplitude of the PPG over a certain period is to calculate the standard deviation (STD) of the PPG signal proportional to its amplitude [26]. Since outliers in the PPG signal are not a useful signal and are almost absent due to small shifts of the study area in the field of view with an almost stationary object, the mean deviation can be replaced by the standard deviation [51]. This study proposes to carry out mapping of PPGSTD in the area of the tumor and surrounding healthy tissues.

Melanin in the epidermis and hemoglobin in the dermis make the main contribution to the absorption of light by the upper layers of the skin [52]. Despite the small differences in the absorption spectra of oxy- and deoxyhemoglobin in the green region of the spectrum [40], it is shown that low-frequency fluctuations in the intensity of radiation scattered by the internal structures of the skin caused by respiration, and, therefore, changes in blood oxygenation can be recorded [36, 50, 53]. We assume that during PDT, changes in the concentration of various forms of hemoglobin, as well as respiration, can lead to fluctuations of the DC-component without any change of other properties of tissues contributing to its value, as well as with fixed lighting. The conversion of various forms of oxygen during PDT is one of the main mechanisms of its action [54]. Therefore, the study provides for mapping changes of DC-components for assessment of the oxygenation.

Experimental animal

The study was conducted on the basis of the laboratory of experimental research of the Center for Laser Medicine of the Pavlov First Saint Petersburg State Medical University in accordance with the Directive 2010/63/EU of the European Parliament and of the Council of 22 September 2010 on the protection of animals used for scientific purposes (Minutes No.100_PF1_112024/27_270).

A Wistar rat (male, weighing 322 g) was used as the object of the study. A strain of the transplanted tumor, cholangioma PC-1, was used to simulate the tumor process. A suspension of tumor tissue was implanted subcutaneously in the area of the outer surface of the right thigh. 21 days after the transplant, the tumor volume was $8.71 \, \text{cm}^3$ (Fig. 1, a).

For photodynamic effects, radachlorin ("Rada-pharma LLC" Russian Federation) was used as a photosensitizer at a dose of 5 mg/kg, which was injected intravenously 3 hours before photoactivation into the tail vein of the animal.

Before photoactivation, the animal underwent anesthesia that comprised an intraperitoneal injection of a mixture of solutions "Zolethyl 100" (Virbac, France) 87.9 mg/kg+"Xyl" (Interchemie, the Netherlands) 17.6 mg/kg. The skin above the tumor node with a capture of at least 1 cm outside the zone of tumor growth was mechanically cleaned of wool. The rat was placed on its left side (with the tumor node facing up) on a thermostatically controlled table TCAT-2LV (Physitemp, USA) with a rectal temperature sensor to monitor the maintenance of constant body temperature during the experiment.

Experimental setup

The experimental setup, designed to visualize and quantify blood microcirculation parameters of skin tumors and surrounding healthy tissues during PDT, has an illumination and imaging channel (Fig. 2). The lighting channel consisted of two LED radiation sources (central wavelength — 520 nm, half-height spectral brightness function width — 30 nm) equipped with Cl collimating lenses to ensure uniform illumination of the studied area.

The imaging channel consists of a lens (Lens) (focal length 18 mm, relative aperture 1:4), a digital color cam-



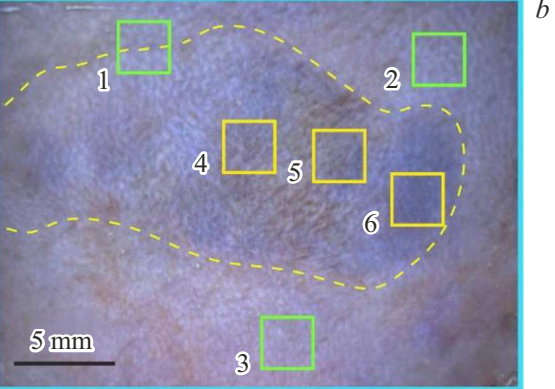


Figure 1. Cholangioma and surrounding tissues: photo (a) and first frame of the image sequence (b) before PDT. The blue square indicates the area of analysis by the proposed method. The dashed line indicates the boundaries of the tumor. Colored squares delimit the tumor areas (4-6) and surrounding tissues (1-3), used to quantify blood microcirculation in them.

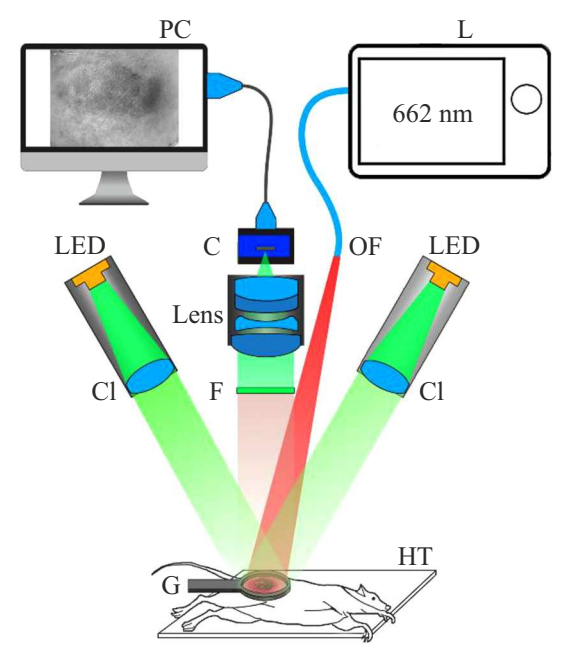


Figure 2. Diagram of the experimental set-up.

era (C) (The Imaging Source DFK33UX252, resolution 2048×1535 pix,pixel size $3.45 \times 3.45 \,\mu\text{m}$, frame rate up to 120 Hz, USB interface 3.0, ADC 12 bit) and a light filter (F) (blocking radiation in the spectral range above $570 \, \text{nm}$), cutting off PA radiation (photoactivation). The lens was placed at a distance of $200 \, \text{mm}$ from the animal and provided an image of both the tumor and surrounding healthy tissues on the sensitive area of the video camera when focusing to infinity. To ensure an equally sharp image across the entire field of view and increase the depth of signal modulation, the study area was covered with a thin glass plate (G).

Laser radiation from PA was transmitted from a laser apparatus (L) ALOD ("Alkom Medica", Russia, 662 nm wavelength) to rat skin using an optical fiber with a microlens (OF) fixed on the imaging channel and providing a diameter of a spot of PA radiation on the tissue under study of 30 mm.

Experiment protocol

The proposed approach and experimental setup were tested during PDT of cholangioma. The studied area of the skin was covered with petroleum jelly oil, which provides enlightenment and a significant reduction in the contribution of the mirror component of reflectivity to image formation, and covered with a glass leveling plate. Next, the backlight was turned on, the system was adjusted to obtain a sharp image of the tumor and surrounding tissues, and a sequence of images with a size of 2048×1535 pix was recorded with a frequency of 50 Hz for 20 seconds (Fig. 1, b). The data obtained during the processing of the recorded sequence was considered the physiological norm for the animal and was taken as a reference.

At the next stage, the PA was conducted in continuous operation for 90 seconds with a power density of 15 mW/cm². Simultaneously with the start of the PA, recording of image sequences was started with the same parameters. The series of 20 s were recorded within 25 min after the start of the experiment.

Data processing

The processing algorithm is shown in Fig. 3. A sequence of monochrome images of the tumor and surrounding healthy tissues was used as input data. During processing, two types of maps were obtained: a change in the DC-component of the recorded signal, proportional to the change in the intensity of radiation backscattered by the internal structures of tissues relative to their initial state (I/I_0) , as well as the spatial distribution of the PPGSTD parameter, proportional to the amplitude of the pulse wave.

At the first stage of processing, the intensity values were averaged in blocks of 3×3 pix for each frame. Despite the decrease in spatial resolution, this technique is traditional for imaging photoplethysmography and makes it possible to eliminate high-frequency spatial interference caused by

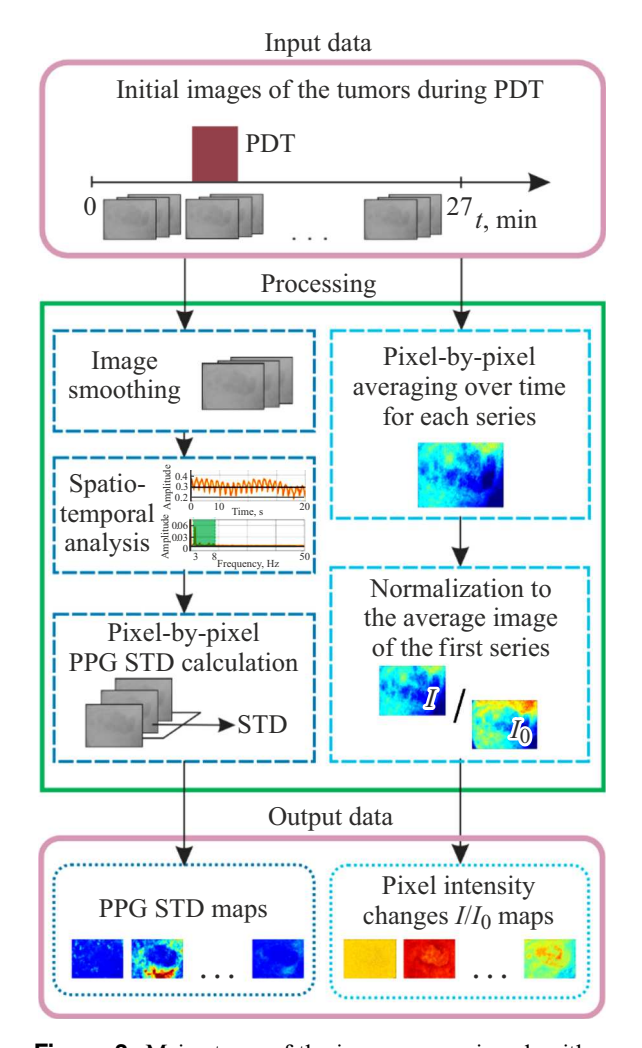


Figure 3. Main stages of the image processing algorithm.

additive noise from the radiation receiver, and increase the signal-to-noise ratio by various estimates from units to tens of times, as well as reduce computing power requirements [44,55]. Each block of 9 pixels corresponded to a signal including AC and DC-components of fluctuations in the intensity of radiation reflected and scattered by the internal structures of the skin, depending, as mentioned earlier, among other things, on blood filling, vasomotor activity of blood vessels, tissue oxygenation, etc.

The ratio I/I_0 was obtained by first averaging the signal in each block of 9 pixels over time over the entire period of recording of frames of a separate series. The obtained spatial distribution of the intensity of reflected and scattered radiation for the first series I_0 reflects the initial optical properties of tissues in the selected spectral range, as well as the spatial unevenness of illumination, i.e. before PDT. Next, the time-averaged images obtained by this method for each series of I were pixel-by-pixel divided into I_0 . It was assumed that the reflectivity, as well as the backlight parameters, remained unchanged in all series. Therefore, the division by I_0 revealed differences in the intensity of radiation scattering to a relative extent. At the same time,

the effect of uneven illumination on the constant component of the signal was eliminated [50,56].

The synthesis of the PPGSTD map was carried out during the spatial-frequency analysis of the array of time signals obtained at the first stage in blocks of 9 pixels. In order to isolate the part of the signal that is modulated by cardiac activity, the Fourier frequency spectrum of the time signal of a separate block, which is traditional for digital signal processing in photoplethysmography, was filtered similarly [24,26,57]. The frequency range corresponding to the useful signal depends on the physiological norm of the animal's heart rate, and for rats it ranges from 3 to 8 Hz in the anesthetized state. The received signal in each block is a PPG and describes to a relative extent periodic fluctuations in the intensity of radiation scattering by the internal structures of the skin attributable to changes in the blood filling of the studied skin area. At the next stage of processing, the PPGSTD parameter was calculated for the time signal in each block, and then the spatial distribution of PPGSTD for the entire image was constructed. To eliminate the effect of uneven illumination, the calculated map was divided into a Gaussian-smoothed image of a uniform white plate similar to Ref. [27,39]. Such PPGSTD maps were obtained for each recorded series of images.

Results and discussion

In the course of an experimental study of the reaction of blood microcirculation of skin tumors and adjacent healthy tissues to photodynamic effects, maps of changes in the intensity of radiation scattered by the studied tissues I/I_0 and PPGSTD. They are shown in Fig. 4 for 5 points of the procedure: before PA (I), at the beginning of PA (II), at the end of PA (III), after 6 min (IV) and after 25 min (V) after the end of PA. The table contains the values of I/I_0 and PPGSTD for three areas inside the tumor, as well as in three areas of surrounding healthy tissues (Fig. 2). The size of the area was $100 \times 100 \, \text{pix}$, which corresponded to about 6 mm². The values in the table are presented in the following format: (average value \pm CO for the selected The values corresponding to the boundaries of the 95% confidence interval are given in the Appendix (Table 1).

The higher intensity of the radiation scattered by the studied tissues corresponds to lower blood filling of tissues and blood oxygenation [19,20]. At the beginning of PA, the scattering intensity (Fig. 4, top row) increased (+7%, p < 0.05), which could be caused by a decrease of the blood oxygenation attributable to the formation of highly reactive singlet oxygen during photodynamic reactions [58]. The greatest increase was observed at the end of PDT at the border of the tumor and healthy tissues and in some areas inside it (+8%, p < 0.05). Healthy tissues showed a decrease in scattering intensity for 6 min after the completion of PDT. At the same time, the achieved scattering intensity values turned out to be lower than

those for the initial states (-5%, p < 0.05), which may be attributable to compensatory reduction processes previously detected by the standard method of laser Doppler flowmetry for PDT analysis [30]. Their relatively high rate of occurrence is due, among other things, to the low radiation power density of PA, and, as a result, relatively small and partially reversible tissue changes [30]. The trend continued by the 25th minute (-10%, p < 0.05). A decrease in scattering intensity relative to the values at the end of PDT was also detected in the first 6 min minutes in the tumor region (-2%, p < 0.05). At the same time, a slight increase in the reflection intensity to $\sim +2\%$ was detected after a local minimum in 6 min. Failure to achieve the initial values may be attributable to the destruction of part of the vascular structures and the inability to sufficiently oxygenate the tissues.

The PPGSTD parameter is proportional to the amplitude of the pulse wave and reflects the change in blood supply to tissues (Fig. 4, bottom row). PPGSTD values are close for skin areas inside and outside the tumor before PA. This parameter slightly increased in the tumor during PDT (+2%, p < 0.05), while in the tissues surrounding the tumor, the change ranged from +10 to $+800\,\%$ during the same period with p < 0.05. Such hemodynamic trends can be explained by a sharp increase in the oxygen supply to the studied tissues and a corresponding increase in blood supply attributable to an increase in vascular density attributable to an increase in transmural pressure in the arterioles [47]. It was previously shown that at low values of the radiation power density PA (1.35,J/cm²), it takes about a minute after the start of irradiation to achieve complete stasis of surface capillaries in healthy tissues [30]. Based on the above, it can be assumed that the main contribution to the identified changes in PPGSTD of healthy tissues is made not by surface capillaries, but by active capillaries in deeper layers of the skin, which lie no deeper than 0.5 mm, i.e. at the depth of penetration of diagnostic radiation into skin tissues, as well as deeper arterioles, pulsation control which in green light is possible in accordance with the model of PPG signal generation [47,49], i.e. attributable to the presence of elastic-mechanical interaction of deep vessels with the dermis. Small changes in the tumor area can be explained by the rapid stasis of blood vessels in it to a greater depth, which prevented an increase in its blood supply.

The presented results demonstrate the potential applicability and usefulness of using imaging photoplethysmography for PDT monitoring, however, for their unambiguous interpretation in terms of the mechanisms of PDT action and widespread use, it is necessary to overcome a number of limitations of the proposed method.

The use of a glass plate leads to an increase in pressure on the area under study, which can affect the amplitudes of the recorded pulse wave [59,60]. The papers provide a theoretical justification for increasing the amplitude of the PPG several times when small forces (of the order of tenths of N/cm²) are applied to the studied area [47,49].

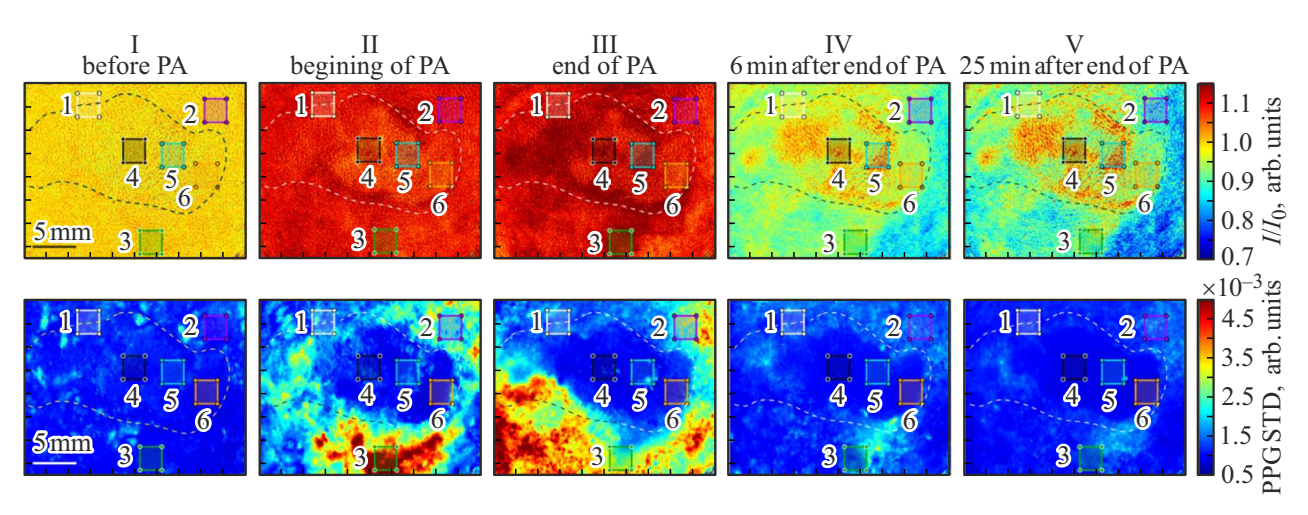


Figure 4. Maps of changes in the intensity of radiation scattered by the internal structures of the studied tissues relative to the initial state I/I_0 (upper row) and PPGSTD (lower row).

The values of the change in the intensity of radiation scattered by the internal structures of the studied tissues relative to the initial state of the tissues I/I_0 and PPGSTD for several areas in the center and on the periphery of the tumor and in the surrounding tissues

Region		Period									
		I before PDT	II at the beginning of PDT	III at the end of the PDT	IV 6 minutes after completion of PDT	V 25 minutes after completion of PDT					
Change of scattering intensity I/I_0											
Outside tumor	1 2 3	0.995 ± 0.116 0.997 ± 0.115 1.001 ± 0.115	$\begin{aligned} 1.063 &\pm 0.123 \\ 1.059 &\pm 0.125 \\ 1.064 &\pm 0.125 \end{aligned}$	$ \begin{aligned} 1.053 &\pm 0.131 \\ 1.055 &\pm 0.127 \\ 1.062 &\pm 0.129 \end{aligned} $	$\begin{array}{c} 0.970 \pm 0.108 \\ 0.964 \pm 0.105 \\ 0.948 \pm 0.111 \end{array}$	$\begin{array}{c} 0.941 \pm 0.130 \\ 0.913 \pm 0.123 \\ 0.877 \pm 0.136 \end{array}$					
Inside tumor	4 5 6	0.994 ± 0.115 0.994 ± 0.115 0.995 ± 0.115	$\begin{array}{c} 1.035 \pm 0.126 \\ 1.044 \pm 0.127 \\ 1.051 \pm 0.127 \end{array}$	$\begin{aligned} 1.052 &\pm 0.129 \\ 1.045 &\pm 0.131 \\ 1.046 &\pm 0.127 \end{aligned}$	0.987 ± 0.115 0.978 ± 0.117 0.965 ± 0.110	$\begin{array}{c} 1.016 \pm 0.138 \\ 0.979 \pm 0.140 \\ 0.996 \pm 0.131 \end{array}$					
Standard deviation of the photoplethysmogram PPGSTD \cdot 10^{-4}											
Outside tumor	1 2 3	8.20 ± 0.71 7.67 ± 0.90 6.14 ± 0.96	$12.57 \pm 5.81 20.33 \pm 2.41 48.55 \pm 1.52$	11.39 ± 2.87 23.81 ± 2.78 24.38 ± 1.33	9.60 ± 1.27 12.29 ± 1.43 11.05 ± 1.13	8.09 ± 1.18 6.29 ± 0.89 8.37 ± 1.20					
Inside tumor	4 5 6	7.06 ± 0.82 6.50 ± 0.76 5.65 ± 0.66	$7.76 \pm 0.91 7.53 \pm 0.93 6.55 \pm 0.87$	5.73 ± 0.68 6.96 ± 0.90 7.38 ± 0.90	5.73 ± 0.67 6.96 ± 0.70 6.05 ± 0.71	$7.48 \pm 1.08 7.07 \pm 1.05 4.57 \pm 0.66$					

This effect is considered as a way to increase the signal-to-noise ratio in the tasks of remotely obtaining the spatial distribution of PPG parameters and is successfully used in a number of biomedical applications [29,61–63]. However, tissue compression can lead to disruption of their blood supply and possible distortion of measurement results. This limitation can be overcome by using a cross-polarization illumination and detection scheme, described in a number of publications, which improves signal quality by reducing the contribution of the radiation component reflected from the upper layers to the detected signal hbox[64–66].

Determining the optimal frame rate of the camera, which ensures reliable signal recording with minimal requirements for computing power and computer memory, may also become one of the areas of future research. The frame rate of the video camera used in this study allowed us to obtain the data (Appendix, Fig. A1), comparable in quality to the signals and their Fourier spectra presented in other papers [52,67].

The selected range of the backlight radiation spectrum increases the signal-to-noise ratio of the recorded signal relative to the results obtained in the red and blue regions,

as mentioned above [43–45], and is widely used in remote detection schemes of PPG [24,25,50]. However, the depth of penetration, and hence the diagnostic volume, with this approach is less than when using the infrared region of the spectrum [40,42]. In addition, the absorption peaks of radachlorin, a common photosensitizer used in the present study, are located in the green region of the spectrum. To overcome this limitation, a combination of the near-infrared and green ranges can be used, which has already shown a significant improvement in the signal-to-noise ratio of the recorded signal and the accuracy of tissue parameter determination based on it [67–69].

During the optimization of the individual components of the stand, it is necessary to evaluate the accuracy and repeatability of the measurements provided by them, while the joint analysis of the recorded data and the results of histological examination of tissues is of interest, similar to Ref. [70], and an increase in the number of studied animals.

The proposed approach made it possible to evaluate individual parameters of blood microcirculation during PDT for the first time simultaneously in a tumor and in surrounding healthy tissues and has significant development prospects taking into account the above limitations. The proposed types of maps can be used to visualize and describe the relative changes in tissue oxygenation and blood supply, which are important for evaluating the effectiveness of PDT [54]. Their simultaneous acquisition and joint analysis will provide additional opportunities for studying the mechanisms of photodynamic effects on microcirculation. The choice of the preferred type of cards is proposed to be carried out in accordance with a specific biomedical task. In the future, it seems useful to use them to analyze PA modes in terms of the interaction of tumor tissues and its environment with different dynamics of depletion of reactive oxygen species in pulsed and continuous PA modes. It is planned to evaluate the reaction of surface vessels in the tumor and compare it with that in healthy tissues under different treatment regimens. A multimodal study of blood microcirculation parameters during PDT using the proposed method and laser Doppler flowmetry, fluorescent and speckle contrast imaging, etc. is also of interest [30,62]. The ultimate goal of such studies is to create a device, as well as to determine diagnostic parameters and quantitative criteria for evaluating the effectiveness of PDT. Such a device is necessary when monitoring the effectiveness of therapy not only for oncological diseases, but also for certain diseases in urology [71], ophthalmology [72], dentistry [73], dermatology [74], etc.

Conclusion

This study describes an experimental bench, a measurement protocol, and a data processing algorithm for visualizing and quantifying the spatial distribution of PPG parameters related to individual parameters of blood microcirculation during PDT. The proposed approach made

it possible to simultaneously map and analyze changes in individual parameters of blood microcirculation during photodynamic exposure and during the period of tissue repair in the tumor and in the surrounding healthy tissues. It is shown that it is possible to determine the spatial distribution of PPGSTD and changes in scattering intensity, providing a relative assessment of changes in blood supply and tissue oxygenation. The developed stand is characterized by its simplicity of technical implementation, non-invasiveness and resistance to changing shooting conditions, which makes it a suitable diagnostic tool for performing many clinical operations. The possibility of conducting research directly during PDT will contribute to obtaining new data on the effect of photodynamic reactions on hemodynamics, as well as the development of new protocols for intraoperative monitoring of the effectiveness of PDT. The limitations of the proposed approach and ways to overcome them, potentially capable of improving measurement accuracy, are described.

Compliance with ethical standards

Experimental studies have been approved by the Bioethics Commission of the Pavlov "First Saint Petersburg State Medical University" of the Ministry of Health of Russia and were carried out in accordance with the European Council Directive (86/609/EEC) on the observance of ethical principles in working with laboratory animals.

Acknowledgments

The results of the work were obtained using the equipment of the Collective Use Center of STC UI RAS [http://ckp.ntcup.ru].

Funding

The study was carried out within the framework of the State Assignment of STC UI RAS (FFNS-2025-0008).

Conflict of interest

The authors declare that they have no conflict of interest.

References

- [1] D. Seth, K. Cheldize, D. Brown, E. E. Freeman. Curr. Dermatol. Rep., 6 (3), 204–210 (2017).
 DOI: 10.1007/S13671-017-0192-7/FIGURES/1
- [2] R.J. Hay, N.E. Johns, H.C. Williams, I.W. Bolliger, R.P. Dellavalle, D.J. Margolis, R. Marks, L. Naldi, M.A. Weinstock, S.K. Wulf, C. Michaud, C.J.l. Murray, M. Naghavi. J. Invest. Dermatol., 134 (6), 1527–1534 (2014). DOI: 10.1038/JID.2013.446
- [3] J. Sun, H. Zhao, L. Fu, J. Cui, Y. Yang. Clin. Cosmet. Investig. Dermatol., 16, 479–498 (2023). DOI: 10.2147/CCID.S401206

- [4] M. Kolarikova, B. Hosikova, H. Dilenko, K. Barton-Tomankova, L. Valkova, R. Bajgar, L. Malina, H. Kolarova. Med. Res. Rev., 43 (4), 717–774 (2023). DOI: 10.1002/MED.21935
- [5] A.G. Niculescu, A.M. Grumezescu. Appl. Sci., 11 (8), 3626 (2021). DOI: 10.3322/CAAC.20114
- [6] J.H. Correia, J.A. Rodrigues, S. Pimenta, T. Dong, Z. Yang. Pharmaceutics, 13 (9), 1332 (2021). DOI: 10.3390/PHARMACEUTICS13091332
- I. Makovik, A. Vinokurov, A. Dunaev, E. Rafailov, V. Dremin. Analyst, 148 (15), 3559–3564 (2023).
 DOI: 10.1039/D3AN00587A
- [8] L.G. Astafyeva, G.A. Zalesskaya, V.Y. Plavskii. Opt. Spectr., 112 (4), 642–647 (2012).
 DOI: 10.1134/S0030400X12040030/METRICS
- [9] P. Agostinis, K. Berg, K.A. Cengel, T.H. Foster, A.W. Girotti, S.O. Gollnick, S.M. Hahn, M.R. Hamblin, A. Juzeniene, D. Kessel, M. Korbelik, J. Moan, P. Mroz, D. Nowis, J. Piette, B.C. Wilson, J. Golab. CA Cancer J. Clin., 61 (4), 250–281 (2011). DOI: 10.3322/CAAC.20114
- [10] A.L. Maas, S.L. Carter, E.P. Wiley, J. Miller, M. Yuan, G. Yu, A.C. Durham, T.M. Busch. Cancer Res., 72 (8), 2079–2088 (2012). DOI: 10.1158/0008-5472.CAN-11-3744/650274/AM/TUMOR-VASCULAR-MICROENVIRONMENT-DETERMINES
- [11] I. Wang, S. Andersson-Engels, G.E. Nilsson, K. Wardell,
 K. Svanberg. British J. Dermatol., 136 (2), 184–189 (1997).
 DOI: 10.1046/J.1365-2133.1997.D01-1166.X
- [12] S. Ohlerth, D. Laluhová, J. Buchholz, M. Roos, H. Walt,
 B. Kaser-Hotz. Lasers Surg. Med., 38 (3), 229–234 (2006).
 DOI: 10.1002/LSM.20282
- [13] M.A. Sirotkina, A.A. Moiseev, L.A. Matveev, V.Y. Zaitsev, V.V. Elagin, S.S. Kuznetsov, G.V. Gelikonov, S.Y. Ksenofontov, E.V. Zagaynova, F.I. Feldchtein, N.D. Gladkova, A. Vitkin. Sci. Rep., 9 (1), 1–9 (2019). DOI: 10.1038/s41598-019-43084-y
- [14] J. Zhu, T. Xiao, J. Zhang, H. Che, Y. Shi, X. Shi, J.C.M. Van Hest. ACS Nano, 14 (9), 11225–11237 (2020). DOI: 10.1021/ACSNANO.0C03080/ASSET/IMAGES/ LARGE/NN0C03080_0005.JPEG
- [15] M. Khurana, E.H. Moriyama, A. Mariampillai, B.C. Wilson. J. Biomed. Opt., 13 (4), 1 (2008). DOI: 10.1111/PHP.13217
- [16] S.C. Hester, M. Kuriakose, C.D. Nguyen, S. Mallidi. Photochem. Photobiol., 96 (2), 260–279 (2020).
 DOI: 10.3390/PHARMACEUTICS14020399
- [17] H. Zuhayri, V.V. Nikolaev, T.B. Lepekhina, E.A. Sandykova, N.A. Krivova, Y.V. Kistenev. Pharmaceutics, 14 (2), 399 (2022). DOI: 10.3390/PHARMACEUTICS14020399
- [18] T.M. Busch, X. Xing, G. Yu, A. Yodh, E.P. Wileyto, H.W. Wang, T. Durduran, T.C. Zhu, K.K.H. Wang. Photochem. Photobiol. Sci., 8 (12), 1683–1693 (2009). DOI: 10.1039/B9PP00004F/METRICS
- [19] J. Allen. Physiol. Meas., 28 (3), R1 (2007). DOI: 10.1088/0967-3334/28/3/R01
- [20] J. Park, H.S. Seok, S.S. Kim, H. Shin. Front. Physiol., 12, 2511 (2022). DOI: 10.3389/FPHYS.2021.808451/BIBTEX
- [21] V.A. Kashchenko, A.A. Kamshilin, V.V. Zaitsev, R.V. Pavlov, A.A. Bogatikov, A.V. Lodigin, O.B. Guschina, N.A. Boyko. Khirurgiia (Sofiia), 9, 33–42 (2023). DOI: 10.17116/HIRURGIA202309233
- [22] A.A. Garanin, V.S. Rogova, P.S. Ivanchina, E.O. Tolkacheva. Reg. blood circ. microcirc., 22 (4), 11–16 (2023). DOI: 10.24884/1682-6655-2023-22-4-11-16

- [23] M. Elgendi, Y. Liang, R. Ward. Diseases, 6 (1), 20 (2018). DOI: 10.3390/DISEASES6010020
- [24] M. Kumar, J.W. Suliburk, A. Veeraraghavan, A. Sabharwal. Sci. Rep., 10 (1), 1–17 (2020). DOI: 10.1038/s41598-020-61576-0
- [25] O.V. Mamontov, A.V. Shcherbinin, R.V. Romashko, A.A. Kamshilin. Appl. Sci., 10 (18), 6192 (2020). DOI: 10.3390/APP10186192
- [26] A.A. Kamshilin, V.V. Zaytsev, A.V. Lodygin,
 V.A. Kashchenko. Sci. Rep., 12 (1), 1–9 (2022).
 DOI: 10.1038/s41598-022-05080-7
- [27] A.S. Machikhin, M.V. Volkov, D.D. Khokhlov, E.D. Lovchikova, A.V. Potemkin, I.V. Danilycheva, I.V. Dorofeeva, A.E. Shulzhenko. Biomed. Opt. Express, 12 (8), 4627–4636 (2021). DOI: 10.1364/BOE.420786
- [28] A.V. Guryleva, A.S. Machikhin, D.D. Khokhlov, M.V. Volkov, V.I. Bukova, M.O. Sharipova, E.V. Orlova, L.M. Smirnova. Proc. SPIE, 12147, 262 (2022). DOI: 10.1117/12.2621479
- [29] A. Guryleva, A. Machikhin, E. Orlova, E. Kulikova, M. Volkov, G. Gabrielian, L. Smirnova, M. Sekacheva, O. Olisova, E. Rudenko, O. Lobanova, V. Smolyannikova, T. Demura. J. Biophoton., e202400242 (2024). DOI: 10.1002/JBIO.202400242
- [30] A.V. Guryleva, A.S. Machikhin, T.G. Grishacheva, N.N. Petrishchev. Biomed. Photonics, 12 (2), 16–23 (2023). DOI: 10.24931/2413-9432-2023-12-2-16-23
- [31] K. Matthes, W. Hauss. Klin. Wochenschr., 17 (35), 1211– 1213 (1938). DOI: 10.1007/BF01778576/METRICS
- [32] A.B. Hertzman. Am. J. Physiol., 124 (2), 328–340 (1938). DOI: 10.1152/AJPLEGACY.1938.124.2.328
- [33] T. Tamura, Y. Maeda, M. Sekine, M. Yoshida. Electronics, 3 (2), 282–302 (2014). DOI: 10.3390/ELECTRONICS3020282
- [34] Y. Maeda, M. Sekine, T. Tamura. J. Med. Syst., 35 (5), 969–976 (2011). DOI: 10.1007/S10916-010-9505-0/TABLES/3
- [35] A.A. Alian, K.H. Shelley. Best Pract. Res. Clin. Anaesthesiol., 28 (4), 395–406 (2014). DOI: 10.1016/J.BPA.2014.08.006
- [36] J. Fine, K.L. Branan, A.J. Rodriguez, T. Boonya-Ananta, A. Ajmal, J.C. Ramella-Roman, M.J. McShane, G.L. Coté. Biosensors, 11 (4), 126 (2021). DOI: 10.3390/BIOS11040126
- [37] H.W. Loh, S. Xu, O. Faust, C.P. Ooi, P.D. Barua, S. Chakraborty, R.S. Tan, F. Molinari, U.R. Acharya. Comput. Meth. Progr. Biomed., 216, 106677 (2022). DOI: 10.1016/J.CMPB.2022.106677
- [38] J. Spigulis. Appl. Opt., 44 (10), 1850–1857 (2005).DOI: 10.1364/AO.44.001850
- [39] A. Guryleva, D. Fomina, M. Volkov, S. Serdoteckova, I. Danilycheva. WECONF-Conf. Proc., (2023). DOI: 10.1109/WECONF57201.2023.10147961
- [40] V. Dremin, E. Zherebtsov, A. Bykov, A. Popov, A. Doronin,
 I. Meglinski. Appl. Opt., 58 (34), 9398–9405 (2019).
 DOI: 10.1364/AO.58.009398
- [41] W.G. Zijlstra, A. Buursma, W.P. Meeuwsen-Van Der Roest. Clin. Chem., 37 (9), 1633–1638 (1991).
 DOI: 10.1093/CLINCHEM/37.9.1633
- [42] A.N. Bashkatov, E.A. Genina, V.I. Kochubey, V.V. Tuchin. J. Phys. D, 38 (15), 2543 (2005).
 DOI: 10.1088/0022-3727/38/15/004
- [43] M.V. Volkov, N.B. Margaryants, A.V. Potemkin, M.A. Volynsky, I.P. Gurov, O.V. Mamontov, A.A. Kamshilin. Sci. Rep., 7 (1), 1–8 (2017).
 DOI: 10.1038/s41598-017-13552-4

- [44] W. Verkruysse, L.O. Svaasand, J. Stuart Nelson, F.P. Wieringa, F. Mastik, A.F.W van der Steen. Opt. Expr., 16 (26), 21434– 21445 (2008). DOI: 10.1364/OE.16.021434
- [45] J. Lee, K. Matsumura, K.I. Yamakoshi, P. Rolfe, S. Tanaka, T. Yamakoshi. Proc. IEEE EMBS, 1724–1727 (2013). DOI: 10.1109/EMBC.2013.6609852.
- [46] R.R. Anderson, J.A. Parrish. Sci. Photomed., 6, 147–194 (1982). DOI: 10.1007/978-1-4684-8312-3_6
- [47] A.A. Kamshilin, E. Nippolainen, I.S. Sidorov, P.V. Vasilev, N.P. Erofeev, N.P. Podolian, R.V. Romashko. Sci. Rep., 5 (1), 1–9 (2015). DOI: 10.1038/srep10494
- [48] N. Sviridova, T. Zhao, K. Aihara, K. Nakamura, A. Nakano. Chaos Sol. Fract., 116, 157–165 (2018). DOI: 10.1016/J.CHAOS.2018.09.016
- [49] A.A. Kamshilin, N.B. Margaryants. Phys. Procedia, 86, 72–80 (2017). DOI: 10.1016/J.PHPRO.2017.01.024
- [50] I.S. Sidorov, L. Babayan, M.A. Volynsky, R. Giniatullin, O.V. Mamontov, A.A. Kamshilin. Biomed. Opt. Expr., 7 (12), 5138–5147 (2016). DOI: 10.1364/BOE.7.005138
- [51] S. Gorard. British J. Ed. Stud., 53 (4), 417–430 (2005).DOI: 10.1111/j.1467-8527.2005.00304.x
- [52] S. Xu, L. Sun, G.K. Rohde. Biomed. Opt. Expr., 5 (4), 1124–1135 (2014). DOI: 10.1364/BOE.5.001124
- [53] L.L. Sánchez-Ramos, B. Morales-Cruzado, F.G. Pérez-Gutiérrez. J. Biomed. Opt., 28 (9), 095002 (2023). DOI: 10.1117/1.JBO.28.9.095002
- [54] G. Yu, T. Durduran, C. Zhou, H.W. Wang, M.E. Putt, H.M. Saunders, C.M. Sehgal, E. Glatstein, A.G. Yodh, T.M. Busch. Clin. Cancer Res., 11 (9), 3543–3552 (2005). DOI: 10.1158/1078-0432.CCR-04-2582
- [55] V.A. Kashchenko, V.V. Zaytsev, V.A. Ratnikov, A.A. Kamshilin. Biomed. Opt. Expr., 13 (7), 3954–3966 (2022). DOI: 10.1364/BOE.462694
- [56] A.S. Machikhin, A.V. Guryleva, V.I. Bukova, D.S. Fomina, G.V. Andrenova. WE-CONF Conf. Proc., (2024). DOI: 10.1109/WECONF61770.2024.10564616
- [57] M. Lai, S.D. van der Stel, H.C. Groen, M. van Gastel, K.F.D. Kuhlmann, T.J.M. Ruers, B.H.W. Hendriks. J. Imag., 8 (4), 94 (2022). DOI: 10.3390/JIMAGING8040094
- [58] T.M. Busch. Lasers Surg. Med., 38 (5), 494–499 (2006). DOI: 10.1002/LSM.20355
- [59] X.F. Teng, Y.T. Zhang. IEEE Trans. Biomed. Eng., 54 (8), 1490–1498 (2007). DOI: 10.1109/TBME.2007.900815
- [60] A. Grabovskis, Z. Marcinkevics, O. Rubenis, U. Rubins, V. Lusa. Photon. Eur., 8427, 104–112 (2012). DOI: 10.1117/12.922649
- [61] M.V. Volkov, A.S. Machikhin, E.D. Lovchikova, D.D. Khokhlov, I.A. Balandin, A.V. Potemkin, V.S. Galanova, I.V. Danilycheva, I.V. Dorofeeva. Sci. Visual., 13 (3), 58–65 (2021). DOI: 10.26583/SV.13.3.06
- [62] V. Dremin, I. Kozlov, M. Volkov, N. Margaryants, A. Potemkin, E. Zherebtsov, A. Dunaev, I. Gurov. J. Biophoton., 12 (6), e201800317 (2019). DOI: 10.1002/JBIO.201800317
- [63] I. Makovik, M. Volkov, L. Eratova, V. Dremin. Opt. Lett., 49 (5), 1137–1140 (2024). DOI: 10.1364/OL.513960
- [64] S. Zaunseder, A. Trumpp, D. Wedekind, H. Malberg. Biomed. Technik, 63 (5), 529–535 (2018).
 DOI: 10.1515/BMT-2017-0119/ASSET/GRAPHIC/J_BMT-2017-0119_FIG_001.JPG
- [65] I.S. Sidorov, M.A. Volynsky, A.A. Kamshilin, J. Henricson, C. Anderson, M.J. Leahy, G.E. Nilsson, F. Sjöberg, T. Wu,

- V. Blazek, H.J. Schmitt. Biomed. Opt. Expr., **7** (7), 2469–2474 (2016). DOI: 10.1364/BOE.7.002469
- [66] S. Guler, O. Ozturk, A. Golparvar, H. Dogan, M.K. Yapici. Phys. Eng. Sci. Med., 45 (4), 1317–1323 (2022). DOI: 10.1007/S13246-022-01175-7/TABLES/1
- [67] A. Trumpp, J. Lohr, D. Wedekind, M. Schmidt, M. Burghardt, A.R. Heller, H. Malberg, S. Zaunseder. Biomed. Eng. Online, 17 (1), 1–19 (2018). DOI: 10.1186/S12938-018-0467-7/FIGURES/9
- [68] A. Moço, W. Verkruysse. J. Clin. Monit. Comput., 35 (1), 123–133 (2021). DOI: 10.1007/S10877-019-00449-Y
- [69] J.P. Sirkiä, T. Panula, M. Kaisti, Advanced Science, 11 (24), 2310022 (2024). DOI: 10.1002/ADVS.202310022
- [70] V.D. Genin, A.B. Bucharskaya, M.Y. Kirillin, D.A. Kurakina, N.A. Navolokin, G.S. Terentyuk, B.N. Khlebtsov, N.G. Khlebtsov, G.N. Maslyakova, V.V. Tuchin, E.A. Genina. J. Biophoton., 17 (4), e202300322 (2024). DOI: 10.1002/JBIO.202300322
- [71] L. Nogueira, A.T. Tracey, R. Alvim, P. Reisz, A. Scherz, J.A. Coleman, K. Kim. Molecules, 25 (22), 5417 (2020). DOI: 10.3390/MOLECULES25225417
- [72] M. Mazloumi, L.A. Dalvin, S.H. Abtahi, N. Yavari, A. Yaghy, A. Mashayekhi, J.A. Shields, C.L. Shields. J. Ophthalmic. Vis. Res., 15 (4), 547 (2020). DOI: 10.18502/JOVR.V15I4.7793
- [73] S.A. Mosaddad, P. Mahootchi, Z. Rastegar, B. Abbasi, M. Alam, K. Abbasi, S. Fani-Hanifeh, S. Amookhteh, S. Sadeghi, R.S. Soufdoost, M. Yazdanparast, A. Heboyan, H. Tebyaniyan, G.V.O. Fernandes. Photobiomod. Photomed. Laser Surg., 41 (6), 248–264 (2023). DOI: 10.1089/PHOTOB.2023.0030
- [74] C.A. Morton, R.M. Szeimies, N. Basset-Séguin, P.G. Calzavara-Pinton, Y. Gilaberte, M. Hædersdal, G.F.L. Hofbauer, R.E. Hunger, S. Karrer, S. Piaserico, C. Ulrich, A.M. Wennberg, L.R. Braathen. J. Eur. Acad. Dermatol. Venereol., 34 (1), 17–29 (2020). DOI: 10.1111/JDV.16044

Translated by A.Akhtyamov

Appendix

Table A1. Values of the change in the intensity of radiation scattered by the internal structures of the studied tissues relative to the initial state of the tissues I/I_0 and PPGSTD for several areas in the center and on the periphery of the tumor and in the surrounding tissues; the average value and the upper and the lower boundaries of the confidence interval (95%) within the region are given

						Period					
Region		I before PDT		II at the beginning of PDT		III at the end of the PDT		IV 6 minutes after completion of PDT		V 25 minutes after completion of PDT	
					Change of scatt	ering inter	nsity I/I_0				
		0.995	0.995 10	1.062	1.062 70	1.052	1.052 30	0.989	0.989 40	0.95849	0.9581 80
	1	12	0.995 14	83	1.062 96	53	1.052 77	64	0.989 88	43	0.9588 08
Outside	2	0.996 66	0.996 63	1.058	1.058 52	1.054	1.054 64	0.964 43	0.964 15	0.91327	0.9129 25
			0.996 68	62	1.058 73	83	1.054 93		0.964 71		0.9136 29
		1.000	1.000	1.064	1.064 22	1.062	1.061	0.947	0.947 18	0.87655	0.8761 22
	3	52	1.000	33	1.064 44	05	1.062	52	0.947 86	5	0.8769
_		0.994	0.994 05	1.035	1.034 90	1.052	1.052	0.987	0.986 90	1.01649	1.0160 47
	4	07	0.994	13	1.035 36	38	1.052 67	31	0.987 72	9	1.0169 51
Inside		0.993	0.993 82	1.043	1.043 35	1.044	1.044	0.977	0.977	0.97945	0.9787 46
tumor	5	85	0.993 88	55	1.043 74	54	1.044 84	88	0.978 23	3	0.9801 59
voillo		0.994	0.994 73	1.051	1.050 90	1.046	1.045 98	0.965	0.964 92	0.99599	0.9957 22
	6	76	0.994 79	09	1.051 29	24	1.046 50	17	0.965 42	6	0.9962 69
			S	tandard d	eviation of the pho	toplethysn	nogram PPGSTD	10^{-4}			
	1	8.20	8.18 8.22	12.57	12.51 12.63	11.39	11.35 11.42	9.60	9.56 9.63	8.09	8.08 8.10
Outside	2	7.67	7.65	20.33	20.26	23.81	23.75	12.29	12.26	6.29	6.26
tumor	3	6.14	7.69 6.13	48.55	20.39 48.49	24.38	23.88	11.05	12.32 11.03	8.37	6.31 8.37
			6.15 7.04		48.62 7.74		24.42 5.70		11.07 5.70		8.38 7.47
	4	7.06	7.08	7.76	7.79	5.73	5.75	5.73	5.75	7.48	7/50
Inside	5	6.50	6.49 6.52	7.53	7.47 7.58	6.96	6.89 7.03	6.96	7.03	7.07	7.06 7.09
tumor	6	5.65	5.64 5.66	6.55	6.49 6.62	7.38	7.34 7.42	6.05	6.03	4.57	4.57 4.58

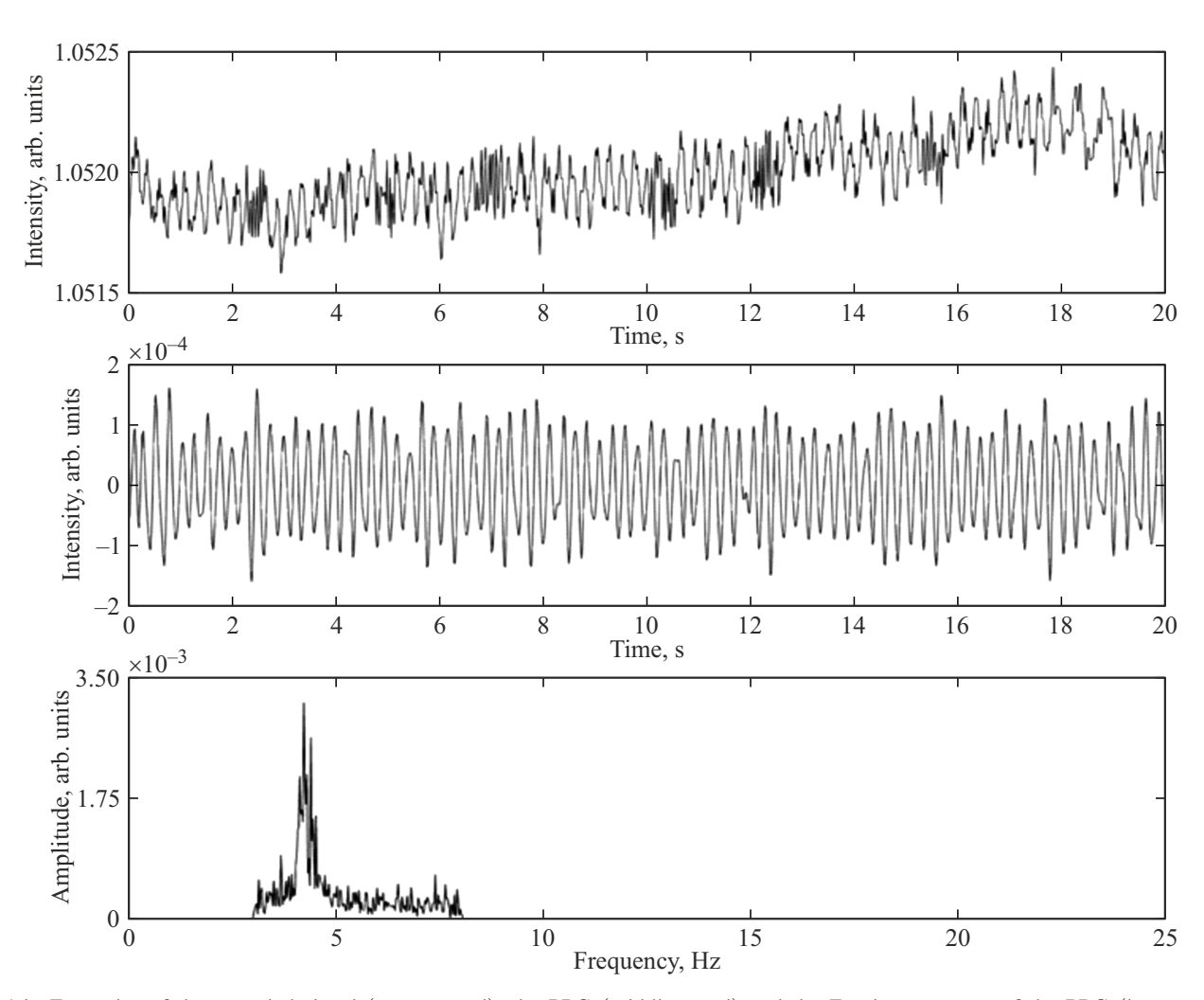


Fig. A1. Examples of the recorded signal (upper panel), the PPG (middle panel) and the Fourier spectrum of the PPG (lower panel) obtained for region 4 in period III (at the end of PA).